PLOS ONE

RESEARCH ARTICLE

Identification of a diguanylate cyclase expressed in the presence of plants and its application for discovering candidate gene products involved in plant colonization by *Pantoea* sp. YR343

Amber N. Bible[1], **Mang Chang**[2], **Jennifer L. Morrell-Falvey**[1,2]*

1 Biosciences Division, Oak Ridge National Laboratory, Oak Ridge, TN, United States of America, **2** UT-ORNL Graduate School of Genome Science and Technology, University of Tennessee, Knoxville, TN, United States of America

* Morrelljl1@ornl.gov

Citation: Bible AN, Chang M, Morrell-Falvey JL (2021) Identification of a diguanylate cyclase expressed in the presence of plants and its application for discovering candidate gene products involved in plant colonization by *Pantoea* sp. YR343. PLoS ONE 16(7): e0248607. https://doi.org/10.1371/journal.pone.0248607

Editor: Seon-Woo Lee, Dong-A University, REPUBLIC OF KOREA

Received: February 26, 2021

Accepted: July 1, 2021

Published: July 21, 2021

Data Availability Statement: All relevant data are within the manuscript and its Supporting Information files.

Funding: This research was sponsored by the Genomic Science Program, U.S. Department of Energy, Office of Science, Biological and Environmental Research, as part of the Plant Microbe Interfaces Scientific Focus Area (http://pmi.ornl.gov). Oak Ridge National Laboratory is managed by UT-Battelle LLC, for the U.S.

Abstract

Microbial colonization of plant roots is a highly complex process that requires the coordination and regulation of many gene networks, yet the identities and functions of many of these gene products have yet to be discovered. *Pantoea* sp. YR343, a gamma-proteobacterium isolated from the rhizosphere of *Populus deltoides*, forms robust biofilms along the root surfaces of *Populus* and possesses plant growth-promoting characteristics. In this work, we identified three diguanylate cyclases in the plant-associated microbe *Pantoea* sp. YR343 that are expressed in the presence of plant roots. One of these diguanylate cyclases, DGC2884, localizes to discrete sites in the cells and its overexpression results in reduced motility and increased EPS production and biofilm formation. We performed a genetic screen by expressing this diguanylate cyclase from an inducible promoter in order to identify candidate gene products that may be involved in root colonization by *Pantoea* sp. YR343. Further, we demonstrate the importance of other domains in DGC2884 to its activity, which in combination with the genes identified by transposon mutagenesis, may yield insights into the mechanisms of plant association as well as the activity and regulation of homologous enzymes in medically and agriculturally relevant microbes.

Introduction

The ability of plant growth promoting bacteria to exert beneficial effects on plant hosts is mediated through chemical and physical associations with plant tissues. Associating with the plant and surviving within this environment likely requires the coordination of multiple signaling pathways. For example, plant colonization involves the second messenger signaling molecule, cyclic diguanylate monophosphate (c-di-GMP), which is known to affect motility, virulence, exopolysaccharide (EPS) production, and biofilm formation in many bacterial

Department of Energy under contract DE-AC05-00OR22725. The funders had no role in study design, data collection and analyses, decision to publish, or preparation of the manuscript.

Competing interests: The authors have declared that no competing interests exist.

species [1–5]. The levels of c-di-GMP within cells are regulated by two different enzymes: diguanylate cyclases, which catalyze the production of c-di-GMP from two molecules of guanosine triphosphate (GTP), and phosphodiesterases, which degrade c-di-GMP to guanosine monophosphate (GMP) [1–3,6]. Most bacterial genomes encode many diguanylate cyclases and phosphodiesterases, suggesting that control of c-di-GMP levels is highly regulated. Production of c-di-GMP by diguanylate cyclases has been shown to modulate a wide variety of cellular behaviors through different types of effector proteins. For instance, the flagellar brake protein, YcgR, from *E. coli* and *Salmonella enterica* serovar Typhimurium, can bind c-di-GMP through a PilZ domain in order to modulate motility [7,8], while the transcriptional regulator, VpsT, regulates biofilm formation in *V. cholera* in response to c-di-GMP levels [9]. Thus far, c-di-GMP has been shown to bind to proteins containing PilZ or GIL domains [10–12], as well as riboswitch proteins [13]. Furthermore, c-di-GMP has also been shown to bind to the RxxD I-sites of many diguanylate cyclases and those with degenerate GGDEF domains often serve as effector proteins [14].

Prior studies have shown that diguanylate cyclases can be regulated at either the level of enzymatic activity or the level of expression, based on conditions within the surrounding environment [1]. Here, we wanted to identify diguanylate cyclases that were regulated at the expression level in the rhizosphere using *Pantoea* sp. YR343. *Pantoea* sp. YR343 was isolated from the rhizosphere of *Populus deltoides* and has been shown to associate with a variety of plant hosts, including *Populus deltoides*, *Populus trichocarpa*, *Triticum aestivum*, and *Arabidopsis thaliana* [15,16]. *Pantoea* sp. YR343 is a gamma-proteobacterium from the *Enterobacteriaceae* family which produces indole-3-acetic acid (IAA) [17,18] and solubilizes phosphate, both of which contribute to plant growth [19]. Furthermore, *Pantoea* sp. YR343 has been shown to form biofilms along the surface of plant roots [15]. Because c-di-GMP plays an important role in biofilm formation, we hypothesized that there may be diguanylate cyclases that are expressed in response to growth in the presence of a plant root. To this end, we identified three diguanylate cyclases in *Pantoea* sp. YR343 that are expressed during colonization of plant roots. Overexpression of one of these diguanylate cyclases (encoded by PMI39_02884 and hereby referred to as DGC2884) significantly impacted EPS production, motility, and biofilm formation. This overexpression strain was utilized for a genetic screen to identify candidate genes that affect the ability of *Pantoea* sp. YR343 to regulate EPS production in the presence of high levels of c-di-GMP which we hypothesized would have defects in biofilm formation and root colonization. Transposon mutants affecting several of these genes were further characterized for their ability to colonize plant roots.

Results

Diguanylate cyclase promoter analysis

The genome of *Pantoea* sp. YR343 contains 13 genes predicted to encode proteins with diguanylate cyclase domains, 8 genes predicted to encode phosphodiesterase domains, 8 genes predicted to encode proteins possessing both diguanylate cyclase and phosphodiesterase domains, and 3 genes predicted to encode proteins with PilZ-domains (https://img.jgi.doe.gov). Table 1 lists each of the diguanylate cyclases found in *Pantoea* sp. YR343, along with its domain organization based on Pfam analyses [20]. Notably, 13 of the 21 predicted diguanylate cyclases lack a canonical RxxD I-site (Table 1). We hypothesized that of the 21 predicted diguanylate cyclases, there were likely some enzymes that were expressed in the presence of a plant. In order to identify candidate enzymes, we began by generating promoter-reporter constructs for each of the 21 genes encoding diguanylate cyclase domains by fusing each promoter to the gene encoding green fluorescent protein (GFP) using a pPROBE-NT vector [21]. Putative

Table 1. Promoter activity under various growth conditions.

DGC[1]	Gene Locus Tag	Domain architecture[2]	liquid culture	biofilm	pellicle	Root colonization[5]
pPROBE	control		1.00	1.00	1.00	-
DGC2884	PMI39_02884	CHASE8-GGDEF	1.16 ± 0.18	1841.20 ± 938.14	1.28 ± 0.17	+
DGC3006	PMI39_03006	PAS3-GGDEF	1.05 ± 0.11	105.44 ± 18.06	1.08 ± 0.18	+
DGC3134	PMI39_03134	MASE5-GGEEF	0.75 ± 0.08	11.76 ± 3.16	1.19 ± 0.44	+
DGC0751	PMI39_00751	dCache_1-GGEEF (RxxD)	0.95 ± 0.12	0.90 ± 0.43	1.03 ± 0.16	-
DGC0995	PMI39_00995	GGEEF	0.95 ± 0.02	5.09 ± 2.37	0.90 ± 0.09	-
DGC1023	PMI39_01023	MHYT-MHYT-MHYT-GGDEF-EAL	1.62 ±0.03	217.99 ±35.02	1.21 ± 0.18	-
DGC1024	PMI39_01024	MHYT-MHYT-MHYT-GGDEF-EAL	0.78 ± 0.02	67.83 ± 28.19	0.98 ± 0.05	-
DGC2242	PMI39_02242	CHASE4-GGDEF-EAL (RxxD)	0.87 ± 0.11	1318.75 ± 112.66	0.93 ± 0.10	-
DGC3247	PMI39_03247	GGEEF (RxxD)	0.94 ± 0.03	24.94 ± 8.30	0.95 ± 0.13	-
DGC3482	PMI39_03482	GAF-GGDEF (RxxD)	0.94 ± 0.02	38.13 ± 9.60	1.20 ± 0.14	-
DGC3621	PMI39_03621	dCache_1-GGEEF (RxxD)	1.27 ± 0.01	22.88 ± 14.83	1.42 ± 0.12	-
DGC0366	PMI39_00366	GAPES4-FRSDF-ELL	5.09 ± 0.69	N. D.[3]	N. D.	N. D.
DGC1008	PMI39_01008	PAS9-PAS9-PAS9-PAS4-GGDEF-EAL (RxxD)	4.35 ± 0.11	N. D.	N. D.	N. D.
DGC1089	PMI39_01089	GGEEF	4.31 ± 0.11	N. D.	N. D.	N. D.
DGC1854	PMI39_01854	MASE1-PAS3-PAS3-PAS-GGDEF (RxxD)	20.95 ± 0.76	N. D.	N. D.	N. D.
DGC2196	PMI39_02196	CHASE7-GGEEF (RxxD)	5.33 ± 0.03	N. D.	N. D.	N. D.
DGC2334	PMI39_02334	GAPES4-GPSDF-EAL	NA[4]	N. D.	N. D.	N. D.
DGC2465	PMI39_02465	CHASE4-PAS-GGDAF-EAL	2.00 ± 0.03	N. D.	N. D.	N. D.
DGC2697	PMI39_02697	PAS9-GGDEF-EAL	16.73 ± 0.27	N. D.	N. D.	N. D.
DGC3217	PMI39_03217	GGEEF	12.77 ± 0.81	N. D.	N. D.	N. D.
DGC4070	PMI39_04070	MASE2-GGDEL	7.76 ± 0.18	N. D.	N. D.	N. D.

Promoter assay performed using pPROBE vector cloned into *Pantoea* sp. YR343 and grown under different conditions. Values for average fluorescence (along with the standard deviation) are reported here. See Materials and Methods for details.

[1]Diguanylate cyclase gene for which the promoter was assayed for activity.

[2]Domain architecture and nomenclature is based on sequence analysis using the Pfam database. (RxxD) indicates that this enzyme possesses a RxxD site.

[3]N. D., not determined.

[4]NA, not available.

[5]Fluorescence was described in qualitative terms, where "+" indicates observed fluorescence and "-" indicates no observed fluorescence.

https://doi.org/10.1371/journal.pone.0248607.t001

gene promoters for each enzyme were predicted using BPROM [22]. We were able to successfully produce these promoter fusion constructs for 20 of the 21 diguanylate cyclases (Table 1). After transforming these constructs into wild type *Pantoea* sp. YR343, the reporter strains were grown to determine under which growth conditions the promoters were active, compared to a control strain carrying an empty pPROBE-NT vector. We measured the average fluorescence intensity of cells grown under various growth conditions and normalized fluorescence intensity values for each reporter strain against the empty vector control strain which we set to a value of 1.00. Reporter strains with weak or no expression (average fluorescence intensity under 2.00; Table 1) when grown in M9 minimal media with 0.4% glucose were chosen for further study in terms of expression in biofilms, pellicles, and during root colonization (Table 1). To test for expression during biofilm formation, the cells were grown statically in M9 minimal medium with 0.4% glucose for 72 hours in 12-well dishes containing a vinyl coverslip as described in Materials and Methods. These data show that eleven diguanylate cyclases showed increased expression under these conditions, with DGC2884 and DGC2242 showing the highest levels (Table 1 and Fig 1). Interestingly, we found that each of the strains showed an increase in expression during biofilm formation based on GFP fluorescence, but images

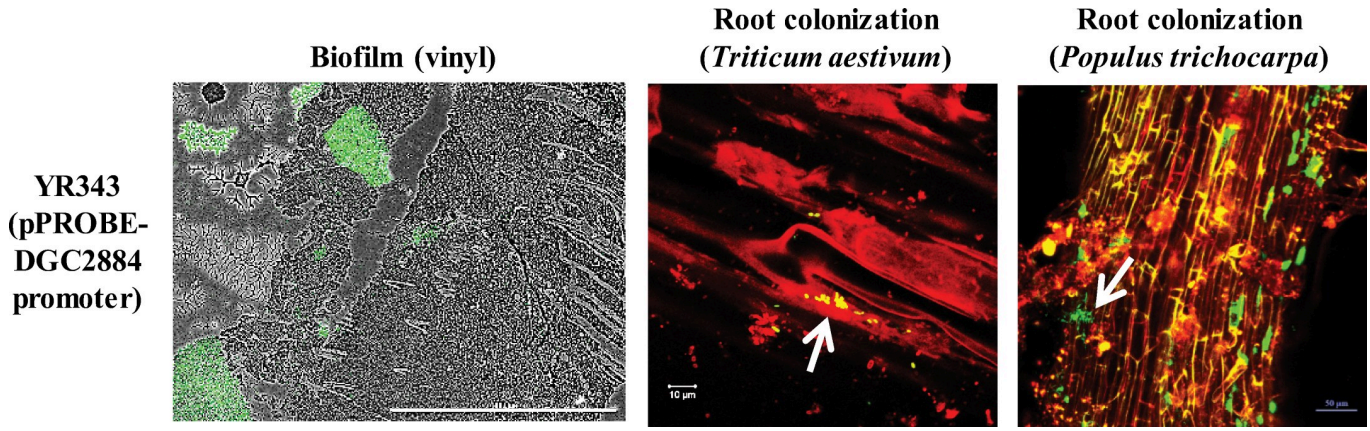

Fig 1. Promoter-GFP reporter assays for DGC2884 expression under different growth conditions: Biofilms on vinyl coverslips, *T. aestivum* root colonization and *P. trichocarpa* root colonization. Scale bars represent 1 mm in biofilm image, while scale bars in root colonization images are labeled accordingly. Arrows indicate bacterial colonization along the surface of plant roots. Data is representative of a minimum of three independent experiments.

https://doi.org/10.1371/journal.pone.0248607.g001

showed that GFP levels driven from the DGC2884 promoter were not uniform within the biofilm (Fig 1). Instead, we found that GFP was highly expressed in specific patches throughout the biofilm, but expressed at low or undetectable levels in other regions. This expression pattern was also observed in some of the other promoter constructs and is reflected, in part, by the higher Standard Error of the Mean (S.E.M.) values shown in Table 1. We also tested for expression during pellicle formation and found that most strains only exhibited a modest increase in expression (Table 1).

Next, we tested the activation of these 12 promoters during root colonization of *T. aestivum and P. trichocarpa* (Table 1). After one week of growth post-inoculation, we found that DGC2884, DGC3006, and DGC3134 were expressed on *T. aestivum* and *P. trichocarpa* roots (Fig 1 and Table 1). We cannot exclude the possibility that the eight untested diguanylate cyclases may also be expressed during plant association since their high levels of background fluorescence during growth in liquid culture precluded testing them directly on plants. For the purpose of this study, however, we chose to focus on DGC2884, which showed strong promoter activity compared to DGC3006 and DGC3134 during biofilm formation, pellicle formation, and in the rhizosphere.

Characterization of DGC2884 and mutant variants in biofilm formation, Congo Red binding, and motility

The domain architecture of DGC2884 lacks a RxxD I-site, and the N-terminal CHASE8 domain of DGC2884 consists of a transmembrane domain and a HAMP (Histidine kinase, Adenylate cyclase, Methyl-accepting protein, and Phosphatase) domain (Table 1). In recent work, it has been suggested that in the absence of a RxxD I-site, the transmembrane and HAMP domains work to dimerize the diguanylate cyclase and allow it to bind to two c-di-GMP molecules and that this function is essential to its enzyme activity [23]. Although efforts to engineer a deletion mutant were unsuccessful, we generated constructs with the full length DGC2884, an enzyme-dead DGC2884 AADEF mutant, and a DGC2884ΔTM mutant and overexpressed each of these in a wild type *Pantoea* sp. YR343 background. Construction and characterization of DGC2884 with the GGDEF motif mutated to AADEF, which has been shown to render diguanylate cyclases enzymatically inactive [23–28], was performed to determine whether enzyme activity was responsible for any observed phenotypes. The

DGC2884ΔTM mutant was constructed to test the hypothesis that the transmembrane domain is essential for function, possibly by facilitating dimerization. Using these constructs, we first examined how expression of DGC2884 and its variants affected colony morphology, Congo Red binding, biofilm formation, and motility in comparison to a control strain carrying an empty vector (Fig 2). Growth curves were compared in both minimal and rich media (S1 Fig). Notably, expression of the wild type, full length DGC2884, but not any of the variants, resulted in formation of small aggregates, likely skewing the measurements of optical density (data not shown). In prior work, we found that *Pantoea* sp. YR343 exhibits a drier colony morphology on LB media and a more mucoid phenotype on R2A media (15); therefore, we first examined growth of these strains on each media type containing Congo Red, a dye specific to β-linked glucans and curli fibers [29]. These results show that *Pantoea* sp. YR343 cells overexpressing DGC2884 (YR343 (pSRK (Km)-*DGC2884*)) resulted in red, wrinkly colony formation (Fig 2A). In contrast, overexpression of the AADEF variant (YR343 (pSRK (Km)-*DGC2884 AADEF*)) resulted in a colony phenotype similar to the empty vector control, with the exception of wrinkles, suggesting that expression of DGC2884 in the absence of enzymatic activity may still retain some function (Fig 2A). We observed reduced Congo Red binding by strains expressing the DGC2884ΔTM variant compared to the DGC2884 expressing strain and we no longer observed wrinkly colony morphology, supporting the hypothesis that the N-terminal transmembrane (TM) domain of DGC2884 is critical to its function (Fig 2A).

Since increased levels of c-di-GMP are typically associated with decreased motility [1,30,31], we next tested whether overexpression of these diguanylate cyclases affected motility using a swim plate agar assay. As expected, overexpression of DGC2884 resulted in impaired motility compared to the control strain, which was partially restored in the DGC2884 AADEF variant (Fig 2B). We found that, in comparison to strains overexpressing DGC2884, expression of DGC2884ΔTM resulted in partial restoration of motility behavior similar to that observed for strains expressing the DGC2884 AADEF mutant (Fig 2B). Together, these data suggest that a fully functional DGC2884 is required to modulate motility.

Next, we examined whether overexpression of these diguanylate cyclases influenced biofilm formation (Fig 2C). While each of these strains showed formation of biofilms on vinyl coverslips, the most robust biofilms were formed during expression of the wild type DGC2884, which was reduced in the DGC2884 AADEF and DGC2884ΔTM mutants (Fig 2C), further indicating the importance of both an active enzymatic site and the N-terminal transmembrane domain. We also tested the effect of overexpression of each diguanylate cyclase variant on pellicle formation by calculating the percentage of cells in pellicles and found that overexpression of DGC2884 resulted in significantly increased pellicle formation when compared to the empty vector control ($p = 0.002$, t-test) (Fig 2D). While expression of DGC2884 AADEF and DGC2884ΔTM resulted in more pellicle formation than the control strain (significantly more by DGC2884ΔTM, $p < 0.029$, t-test), they produced significantly less pellicle than that of wild type cells overexpressing the full-length DGC2884 ($p = 0.012$ for DGC2884 AADEF; $p = 0.004$ for DGC2884ΔTM), both of which were measured by the student's t-test. ANOVA analysis showed a p-value of 0.007 between groups in this experiment (Fig 2D).

Lastly, we assessed the enzyme activity of wild type DGC2884 and the DGC2884ΔTM and DGC2884 AADEF mutants using a Vc2-Spinach aptamer which acts as a c-di-GMP biosensor [32]. For this assay, the full length DGC2884 diguanylate cyclase and each of the variants were expressed in *E. coli* BL21 DE3 Star cells and the fluorescence intensity of cells was measured as an indicator of c-di-GMP levels (Fig 2E and 2F). Indeed, we found that cells expressing DGC2884 had significantly higher fluorescence intensity compared to control cells, consistent with DGC2884 being an active diguanylate cyclase. Furthermore, cells expressing the DGC2884 AADEF variant were significantly less fluorescent than cells expressing DGC2884,

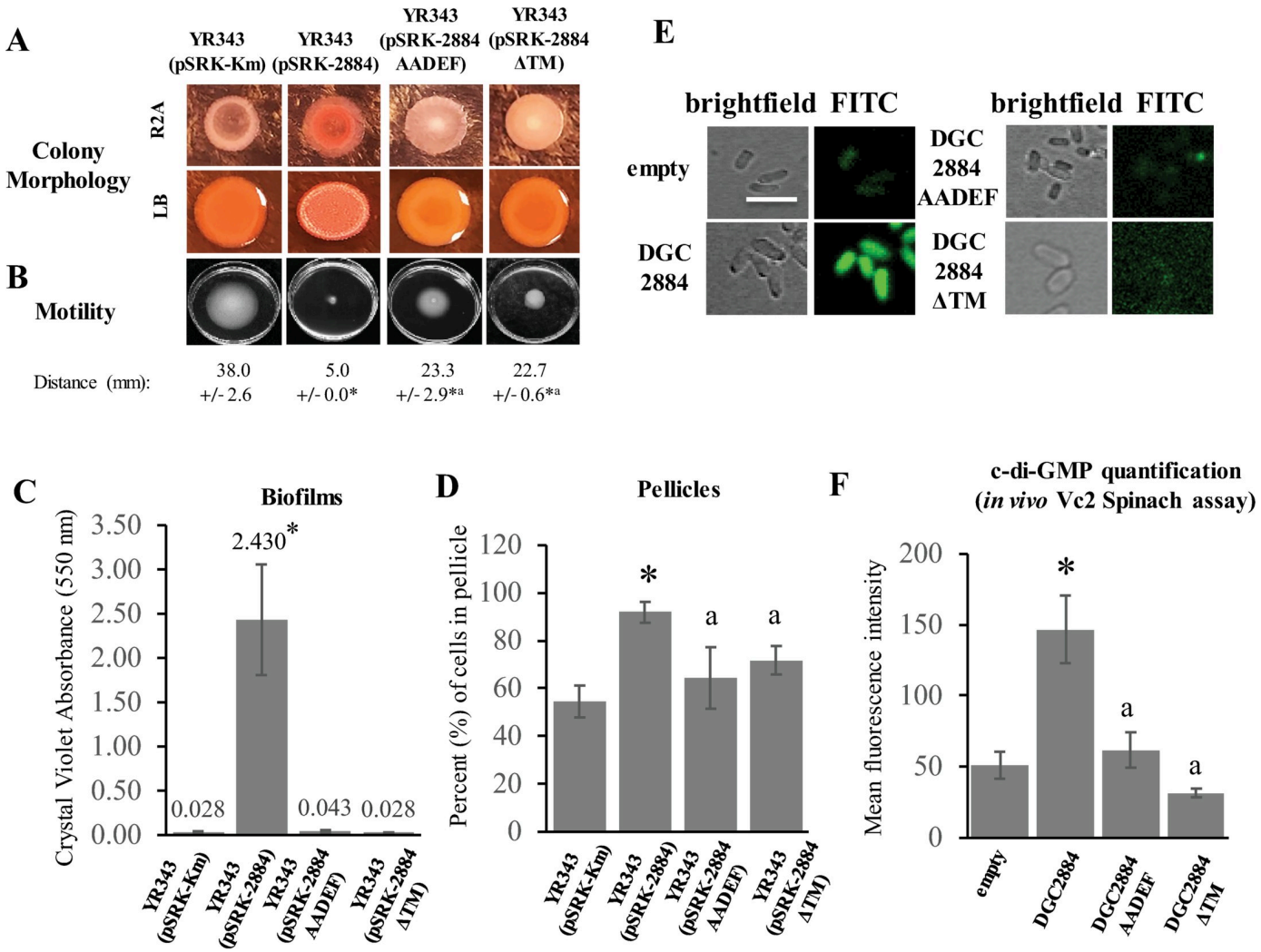

Fig 2. Characterization of individual diguanylate cyclases expressed in a wild type *Pantoea* sp. YR343 background. (A) Indicated strains were spotted on either LB or R2A media containing Congo Red for 48 hours prior to imaging. Each plate consisted of three replicates and experiments were repeated at least three times. (B) Swim agar plates were inoculated in the center of each plate and incubated for 24 hours prior to imaging. Average swimming ring diameter was determined from three individual experiments consisting of three biological replicates each. (*) indicate statistically significant differences ($p \leq 0.001$) compared to the wild type strain harboring an empty vector and ([a]) represents statistically significant differences ($p \leq 0.001$) compared to the strain overexpressing DGC2884, both of which were measured by the student's t-test. ANOVA analysis also showed significant differences between samples with a p-value ≤ 0.001. (C) Indicated strains were grown under conditions conducive to biofilm formation on vinyl coverslips for 72 hours prior to staining with Crystal Violet. Average absorbance values at 550 nm for each sample are shown in graph. Data is representative of at least three independent experiments consisting of at least 3 biological replicates per sample each time. (*) indicate statistically significant differences ($p < 0.005$) as measured by the student's t-test when compared to the wild type strain with the empty vector. ([a]) represents a statistically significant difference ($p < 0.001$) when compared to overexpression of DGC2884 as measured by the student's t-test. ANOVA statistical analysis also showed significant differences between samples ($p \leq 0.001$). (D) Pellicle formation assays were used to compare the percentages of cells in pellicles for each sample after a period of 72 hours. Each bar represents three biological replicates from a single experiment. Experiment was performed twice with similar results. (*) indicate statistically significant differences ($p = 0.002$) compared to the wild type strain possessing an empty vector and (a) represents a statistically significant difference ($p = 0.012$ for DGC2884 AADEF; $p = 0.004$ for DGC2884ΔTM) compared to the strain overexpressing DGC2884, both of which were measured by the student's t-test. ANOVA analysis showed a p-value of 0.007 between groups in this experiment. (E) Fluorescence micrographs of representative cells co-expressing the Vc2 Spinach aptamer with the indicated constructs. Scale bar represents 5 μm. (F) Diguanylate cyclase enzyme activity is shown as a bar graph comparing the mean fluorescence intensity measured across 50 cells per sample. Error bars represent the S.E.M. values. (*) indicate statistically significant differences ($p < 0.001$) as measured by the student's t-test. ANOVA analysis showed significant differences between groups ($p \leq 0.001$). Data shown represents three separate experiments.

https://doi.org/10.1371/journal.pone.0248607.g002

suggesting that the AADEF mutation indeed affected enzyme activity (Fig 2E and 2F). We also found that cells expressing DGC2884ΔTM had little to no fluorescence (Fig 2E and 2F).

Expression of these constructs in cells was verified by RT-PCR (S2 Fig). Taken together, results from each of these assays confirm that both enzyme activity and the N-terminal transmembrane domain are critical to the function of DGC2884.

Domain architecture and role of transmembrane domain in localization pattern of DGC2884

To gain further insight into the function of DGC2884, we examined localization of DGC2884 and DGC2884ΔTM in a wild type background by expressing it fused to either a 3HA or 13Myc tag (Fig 3). These data show that DGC2884 was localized primarily in discrete foci at the cell pole or towards the mid-cell. In the absence of the N-terminal transmembrane domain, however, DGC2884 no longer localized as discrete foci, but rather the localization pattern became more diffuse with fewer visible foci (Fig 3B and Table 2). To verify that the tag did not alter the expression or function of these enzymes, we performed a motility assay (Fig 3C) and western blot (S3 Fig) and observed that each construct was expressed and functional compared to a control strain harboring the same vector backbone but with *ipdC* inserted in place of the diguanylate cyclase gene. From previous work, expression of *ipdC*, which encodes indole pyruvate decarboxylase, did not affect motility in *Pantoea* sp. YR343 [17].

Identification of genes affected in colony morphology and Congo Red binding under high c-di-GMP levels using transposon mutagenesis

Overexpression of DGC2884 resulted in a number of phenotypes (shown in Fig 2), including wrinkly colonies, increased Congo Red binding, increased pellicle and biofilm formation, and decreased motility, all of which suggest that DGC2884 is an active enzyme that influences c-di-GMP levels. Because expression of this diguanylate cyclase is influenced by plant association, we wanted to examine the molecular basis for the observed effects of DGC2884 expression on *Pantoea* behavior. To this end, we designed a transposon mutant screen to identify mutants that failed to respond to high levels of c-di-GMP resulting from DGC2884 overexpression, as determined by differences in Congo Red binding compared to the wild type strain overexpressing DGC2884. For this screen, we constructed a small transposon mutant library in *Pantoea* sp. YR343 (pSRK (Gm)–*DGC2884*) and screened for mutants of interest by plating the library on R2A plates containing Congo Red. Colonies that did not display the typical DGC2884 overexpression phenotype of wrinkled colonies and/or increased Congo Red binding were selected for further analyses. From this screen, we isolated 136 mutants that failed to respond to DGC2884 overexpression. Using a rescue cloning approach, we identified the location of the transposon insertion in each of these mutants, which resulted in a list of 58 genes, with some genes represented by multiple transposon mutants (Table 3). The top 5 COG (Clusters of Orthologous Groups) categories represented among this set of genes include transcription (K), signal transduction (T), cell wall/membrane/envelope biogenesis (M), carbohydrate transport and metabolism (G), and intracellular trafficking/secretion/vesicular transport (U). We also identified 15 genes that were classified as either hypothetical proteins or that were not in a COG category.

Behavioral defects observed in selected mutants

Using the list of genes found in the genetic screen (Table 3), we selected eight different transposon mutants with diverse predicted functions for further analyses, including a predicted UDP-galactose lipid carrier transferase (PMI39_01848; UDP::Tn5) and a predicted capsule polysaccharide transporter (PMI39_03059; CAP::Tn5), both of which have a predicted role in

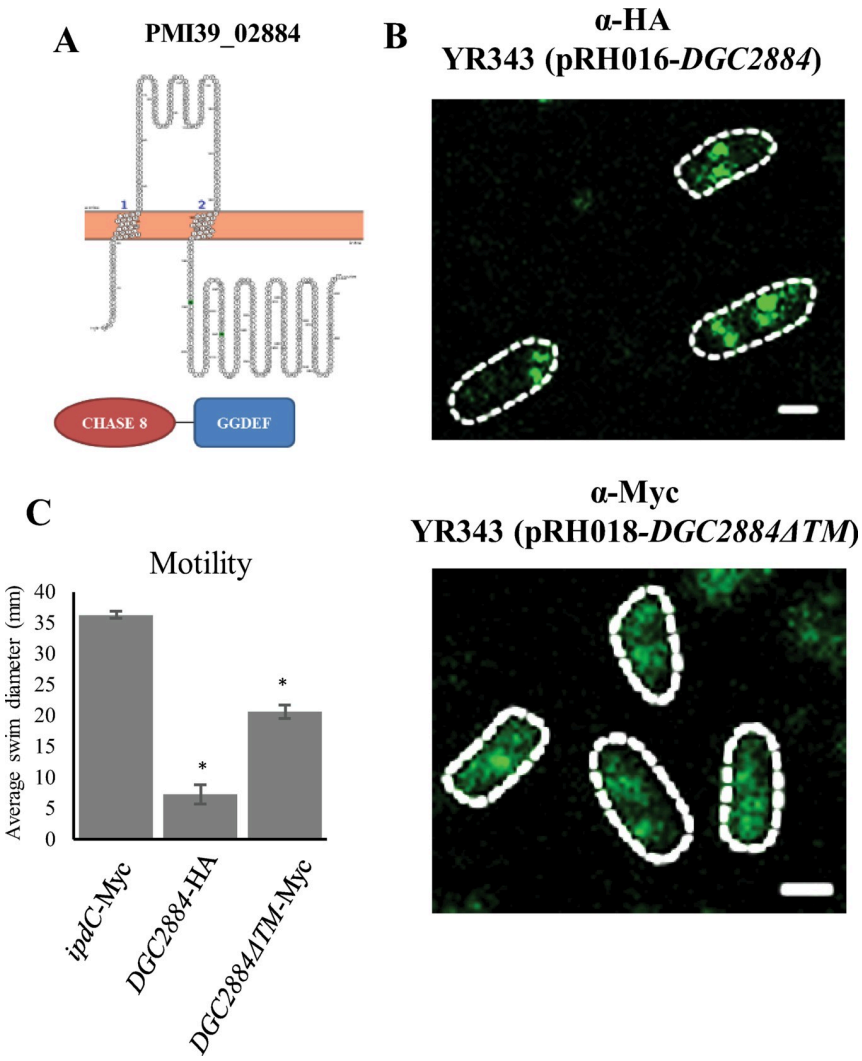

Fig 3. Localization of wild type DGC2884 and DGC2884ΔTM expressed in a wild type background using immunofluorescence assays. (A) Predicted topological structure of DGC2884 using Protter (top) and domain organization based on pfam analysis (bottom). (B) HA- tagged DGC2884 and Myc-tagged DGC2884ΔTM were detected using immunofluorescence assays and imaged using confocal microscopy. Individual cells are outlined in a white dashed line. Scale bars represent 1 μm. (C) Motility plate assays demonstrating functionality of tagged constructs, including an *ipdC* negative control. Data represent three biological replicates and at least two independent experiments. (*) indicate statistically significant differences ($p < 0.001$) as measured by the student's t-test. ANOVA analysis also showed statistically significant differences between samples ($p \leq 0.001$).

https://doi.org/10.1371/journal.pone.0248607.g003

Table 2. Quantification of GFP localization for tagged diguanylate cyclases.

		Cells with indicated number of foci (%)					
DGC	**total cells (n)**	**diffuse/no foci**	**1**	**2**	**3**	**4**	**5**
2884	55	0	42	33	16	9	0
2884ΔTM	101	55	20	13	2	0	11

Images from Fig 3 were analyzed with Fiji ImageJ software to assess localization of indicated proteins. Foci were counted per cell and populations consisting of different localization patterns were placed into the indicated categories and population percentages were reported.

https://doi.org/10.1371/journal.pone.0248607.t002

Table 3. List of genes identified by transposon mutagenesis.

Locus tag	Gene Product Name	COG Category	Number of hits
PMI39_00157	integrase	L	1
PMI39_00228	Hypothetical protein		1
PMI39_00241	hypothetical protein wp_008101727		1
PMI39_00454	alpha/beta hydrolase	R	1
PMI39_00487	AMP-binding protein	I	1
PMI39_00509	transcriptional regulator	K	3
PMI39_00617	succinate-semialdehyde dehydrogenase	C	1
PMI39_00716	ligand-gated channel protein	P	1
PMI39_00827	diguanylate phosphodiesterase	T	1
PMI39_00954	hypothetical protein		1
PMI39_00979	succinylornithine aminotransferase	E	2
PMI39_01013	Response regulator	K T	1
PMI39_01243	hypothetical protein		2
PMI39_01268	DEAD/DEAH box helicase	V	1
PMI39_01302	hypothetical protein		1
PMI39_01645	short-chain dehydrogenase	I Q R	1
PMI39_01786	histidine kinase	T	1
PMI39_01848	UDP-phosphate galactose phosphotransferase	M	1
PMI39_01849	membrane protein TerC	P	1
PMI39_01865	lipid kinase	R I	3
PMI39_01945	hypothetical protein		1
PMI39_01946	hypothetical protein		2
PMI39_01962	ATP-binding cassette, subfamily C, LapB	V	1
PMI39_01991	transcriptional regulator	K	1
PMI39_02071	xylose ABC transporter substrate-binding protein	G	5
PMI39_02188	flagellar biosynthesis protein FliR	N U	47
PMI39_02189	Response regulator containing a CheY-like receiver domain and an HTH DNA-binding domain	K T	4
PMI39_02190	methyl-accepting chemotaxis protein	N T	1
PMI39_02310	integrase	L	1
PMI39_02350	UDP-N-acetyl-D-mannosamine dehydrogenase	M	1
PMI39_02416	bilin biosynthesis protein CpeZ	K	1
PMI39_02667	peptide ABC transporter substrate-binding protein	E	1
PMI39_02700	L-ribulose-5-phosphate 4-epimerase	G	1
PMI39_02775	membrane protein	S	1
PMI39_02840	2-methylcitratede hydratase		1
PMI39_03014	dienelactone hydrolase	Q	1
PMI39_03048	endonuclease	L	1
PMI39_03059	Capsule polysaccharide transporter	M	1
PMI39_03065	hypothetical protein		3
PMI39_03156	Protein of unknown function (DUF3274)		1
PMI39_03162	type VI secretion protein ImpG		1
PMI39_03169	glyceraldehyde-3-phosphate dehydrogenase	G	1
PMI39_03186	hypothetical protein wp_008107569		2
PMI39_03244	nitrate reductase	C	1
PMI39_03380	channel protein TolC	M U	1
PMI39_03579	nucleoside-diphosphate kinase	F	2
PMI39_03698	deoxyguanosinetriphosphate triphosphohydrolase	F	2

(*Continued*)

Table 3. (Continued)

Locus tag	Gene Product Name	COG Category	Number of hits
PMI39_04079	hypothetical protein		1
PMI39_04218	urea ABC transporter	E	1
PMI39_04305	signal transduction histidine kinase	T	3
PMI39_04393	glycerol uptake facilitator GlpF	G	2
PMI39_04394	glycerol uptake facilitator GlpF	C	1
PMI39_04442	hypothetical protein		1
PMI39_04512	cell division protein FtsY	U	1
PMI39_04570	transposase		1
PMI39_04700	Outer membrane autotransporter barrel domain-containing protein	M U	2
PMI39_04978	ABC transporter ATP-binding protein	P	5
PMI39_04984	hypothetical protein	D	1

https://doi.org/10.1371/journal.pone.0248607.t003

exopolysaccharide production. Because approximately one third of the identified transposon mutants were affected in *fliR* (PMI39_02188; FliR::Tn5), we included this mutant for further characterization as well. We also chose mutants predicted to be affected in Type VI secretion (PMI39_03162; Type VI::Tn5), in glycerol uptake (PMI39_04394; GlpF::Tn5), transport (PMI39_04218; ABC::Tn5), a nucleoside-diphosphate kinase (PMI39_03579; Ndk::Tn5), and one of the twelve hypothetical proteins (PMI39_03065; Hypo::Tn5). We began by curing each mutant of the DGC2884 expression plasmid (pSRK(gm)-*DGC2884*) in order to introduce an empty pSRK(gm) vector control prior to examining EPS production (by observing phenotypes on media with Congo Red) (Fig 4A and 4B). Next, we used the cured transposon mutants to observe pellicle formation (Fig 4C), and measured biofilm production with a crystal violet assay (Fig 4D). Compared to the wild type control, each mutant had a different growth phenotype on media with Congo Red, some of which were more noticeable on one media type over the other (Fig 4A and 4B). These phenotypes were further influenced based on whether the mutant expressed DGC2884 (pSRK (gm)-*DGC2884*) or an empty vector (pSRK (gm)). We next examined the effects of these mutations on pellicle formation and found that the UDP::Tn5, FliR::Tn5, and GlpF::Tn5 mutants produced significantly less pellicle than the wild type strain (Fig 4C). We also examined biofilms attached to vinyl coverslips and found that while some mutants appear to produce more biofilm, such as FliR::Tn5 and GlpF::Tn5, there were no statistically significant differences measured by quantifying Crystal Violet staining. Interestingly, we did find that the UDP::Tn5 and Ndk::Tn5 mutants produced significantly more biofilm than the wild type strain in this assay (Fig 4C).

Finally, we examined the colonization behavior of each mutant on *Populus* plant roots. These data showed that the UDP::Tn5 mutant showed significantly reduced colonization compared to the wild type strain, while the Type VI::Tn5, ABC::Tn5, and Ndk::Tn5 mutants showed a slight, though significant, increase in colonization (Fig 5A; statistically significant differences with $p < 0.001$ for UDP::Tn5 and Type VI::Tn5 compared to the wild type and $p = 0.002$ for ABC::Tn5 and Ndk::Tn5 compared to the wild type using the student's t-test. ANOVA analysis indicated statistically significant differences between samples with a p-value below 0.001). Comparisons of growth rates between transposon mutants and the wild type strain showed no significant differences for most strains, except for growth with UDP::Tn5 which was slightly affected compared to the wild type (S4 Fig) and may contribute, in part, to the observed two orders of magnitude reduction in colonization.

In addition to counting the overall number of microbes, we also wanted to determine how these mutant strains were distributed along the plant roots during colonization compared to

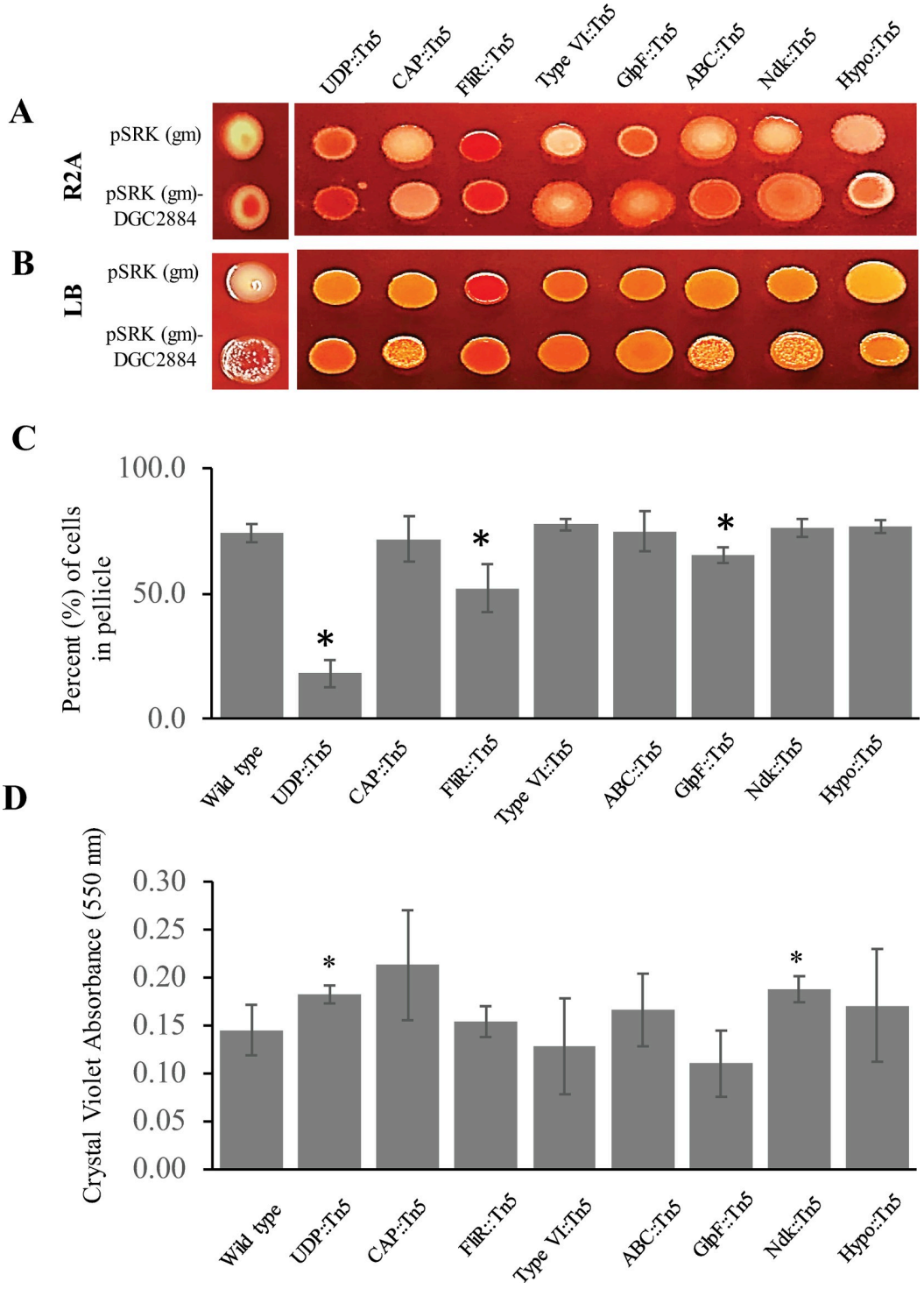

Fig 4. Characterization of behavioral defects among selected transposon mutants: UDP::Tn5 (PMI39_01848), CAP::Tn5 (PMI39_03059), FliR::Tn5 (PMI39_02188), TypeVI::Tn5 (PMI39_03162), GlpF::Tn5 (PMI39_04394), ABC::Tn5 (PMI39_04218), Ndk::Tn5 (PMI39_03579), and Hypo::Tn5 (PMI39_03065). Individual strains possessing either an empty pSRK-gm vector or pSRK(gm)-DGC2884 were spotted onto R2A (A) or LB (B) plates with Congo Red and incubated for 48 hours prior to imaging. (C) Each strain was grown under conditions conducive to pellicle formation for 72 hours. Graph indicates the average percentage of cells within the pellicles taken from three biological replicates. (*) indicate statistically significant differences ($p < 0.001$ for UDP::Tn5, $p = 0.007$ for FliR::Tn5, and $p = 0.016$ for GlpF::Tn5) when compared to the wild type strain using the student's t-test. ANOVA analysis showed a statistically significant difference

between groups with a p-value below 0.001. (D) Biofilm assays were performed using vinyl coverslips for 72 hours prior to staining with crystal violet. Bar graphs describe the average absorbance at 595 nm per sample as determined from two experiments, each with a set of three biological replicates. (*) indicates statistically significant differences (p-value = 0.043 for UDP::Tn5; p-value = 0.033 for Ndk::Tn5) when compared to the wild type strain using the student's t-test. ANOVA analysis showed a p-value of 0.179 between groups for this assay.

https://doi.org/10.1371/journal.pone.0248607.g004

wild type. For our studies, the wild type strain, the UDP::Tn5, and CAP::Tn5 mutant were each tagged with green fluorescent protein to facilitate imaging. The remaining mutants were observed by staining with Syto 9 dye (Fig 5B). In recent work by Noirot-Gros *et al.* [33], several patterns of root surface colonization in Aspen were described to facilitate comparisons,

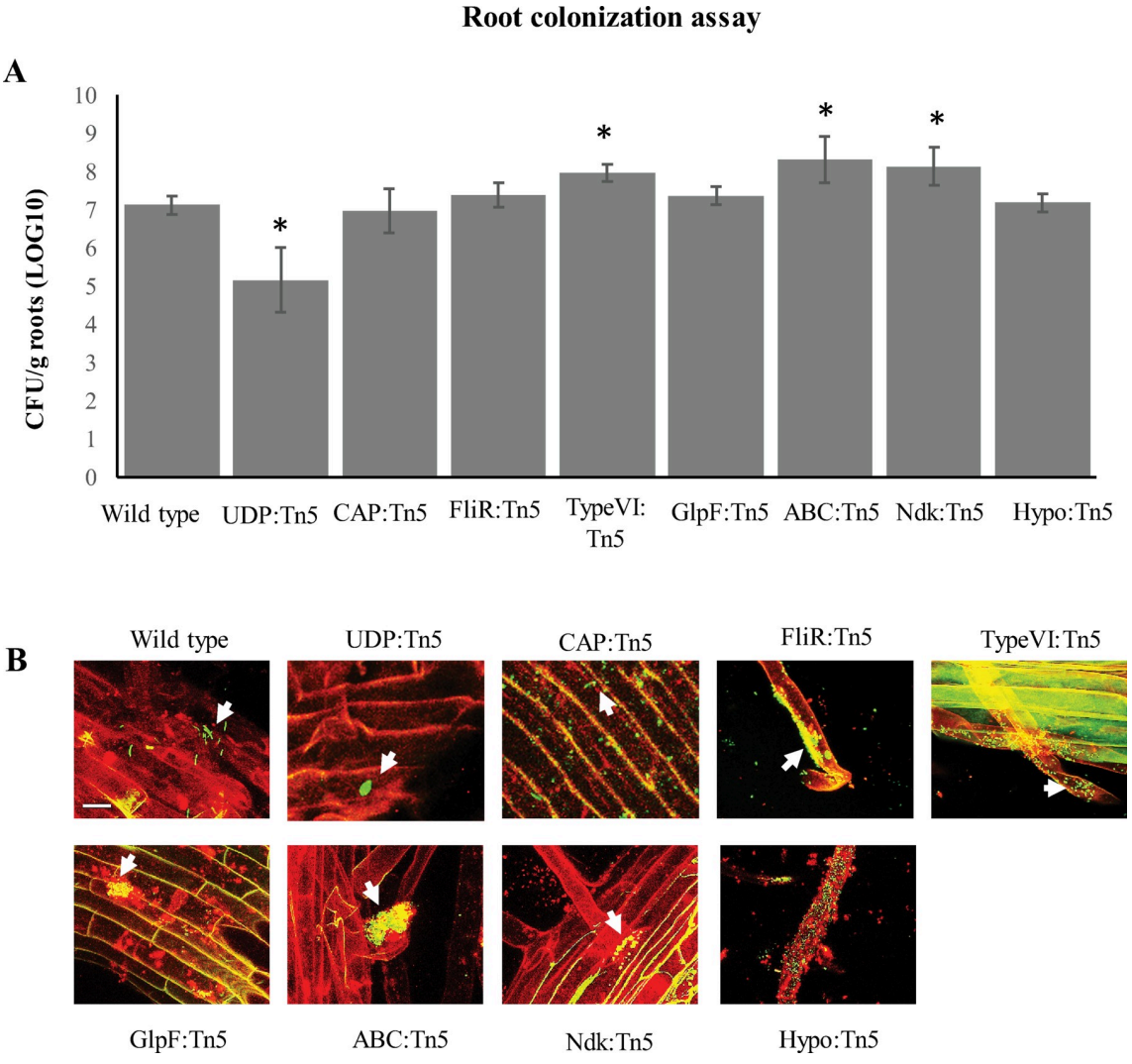

Fig 5. Effects of transposon mutations on root colonization patterns in *P. trichocarpa*. (A) Colonization of plant roots inoculated with wild type *Pantoea* YR343, UDP::Tn5, CAP::Tn5, FliR::Tn5, Type VI::Tn5, GlpF::Tn5, ABC::Tn5, Ndk::Tn5, or Hypo::Tn5 mutants and was measured after 3 weeks by counting CFUs relative to the total weight of each plant root. Error bars represent standard deviation over three to five different biological replicates per sample and (*) represent statistically significant differences ($p < 0.001$ for UDP::Tn5 and Type VI::Tn5 compared to the wild type and $p = 0.002$ for ABC::Tn5 and Ndk::Tn5 compared to the wild type using the student's t-test. ANOVA analysis indicated statistically significant differences between samples with a p-value below 0.001). (B) Images of *P. trichocarpa* (red) one week after inoculation with the indicated bacterial strains (green). Scale bar represents 10 μm.

https://doi.org/10.1371/journal.pone.0248607.g005

including no pattern (NP), long strips (LS), long patch microcolonies (LP), short patch microcolonies (SP), and high density bacterial coating (C). Using these descriptions, we observed that wild type *Pantoea* sp. YR343 exhibited a combination of long strips, long patch microcolonies, and small patches and was localized along the main root and root hair regions (Fig 5B). Consistent with its reduced counts, it was difficult to detect the UDP::Tn5 mutant on the root surface, although some small patches along the primary root surface were observed. The colonization pattern of CAP::Tn5 was very different from wild type, even though the overall level of colonization was similar (Fig 5B). Interestingly, the CAP::Tn5 mutant did not display a pattern of any kind, but was spread out over the root surface as individual cells and did not form patches like the wild type strain, possibly indicating a role of EPS in modulating the physical patterns of colonization along plant roots. Colonization by the FliR::Tn5, Type VI::Tn5, ABC::Tn5, and Hypo::Tn5 mutants consisted of long strips and small patches of cells and were found predominantly along the root hairs (Fig 5B). Both the Ndk::Tn5 and GlpF::Tn5 mutants exhibited primarily small patches of cells which appeared to be quite spread out along the main root, but near root hair regions (Fig 5B). Among these transposon mutants, the strains with the most noticeable differences in colonization patterns were CAP::Tn5, Ndk::Tn5, and GlpF::Tn5.

Discussion

We describe here the identification of three diguanylate cyclases in *Pantoea* sp. YR343 that were expressed consistently during colonization of plant roots. Although we only identified three diguanylate cyclase genes (out of 21 predicted genes) that are expressed in the presence of plants, it is possible that the nature of this assay may have excluded other potential genes of interest. For example, predicted promoter sites may have been incorrect or some genes may have been expressed at earlier or later times during colonization. Further, some of the diguanylate cyclases that were not tested due to high initial fluorescence (over 2.00) under laboratory growth conditions may have important roles during plant colonization. To date, we know of only one other diguanylate cyclase, Chp8 from *Pseudomonas syringae* pv. Tomato DC3000, that is activated in the presence of plants and appears to be involved in reducing flagellin expression, increasing EPS production, and avoiding plant immune responses [34]. Interestingly, the ability to suppress flagellar gene expression is a key strategy in avoiding plant immune responses since flagellin is a common pathogen-associated molecular pattern (PAMP) protein [35]. While this appears to be a common strategy among plant pathogens for host invasion, there have been only a few reports describing the role of c-di-GMP in these processes [36].

We focused our characterization studies on DGC2884 which exhibited the most dramatic phenotypes when overexpressed, including modulating EPS production, motility, and biofilm formation. Our data indicates that the N-terminal CHASE domain of DGC2884 appears to be necessary for localization and enzyme function. The presence of CHASE domains within various proteins, including diguanylate cyclases, have been described as having different sensory capacities [37–40], though precisely what these domains sense is still unknown. We found that the full-length DGC2884 localized as discrete foci within the cell, suggesting that this enzyme may influence local concentrations of c-di-GMP or may localize in order to yield specificity in its downstream effects. DGC2884 also lacks the regulatory RxxD I-site. In the absence of an I-site, the two glycine residues in the GGDEF domain are essential for binding of c-di-GMP [23]. Interestingly, this domain architecture is not altogether unusual and has been studied in other enzymes. The best studied diguanylate cyclases with these domains are YfiN (or TpbB) from *Pseudomonas aeruginosa*, *Salmonella enterica*, and *Escherichia coli* (also called DgcN)

[7,41–43]. These enzymes have been shown to primarily regulate motility via YcgR and production of exopolysaccharides (such as Pel and Psl in *P. aeruginosa*), in addition to roles in cell division [7,41–43]. Among these examples, DgcN from *E. coli* is the only example to lack a RxxD I-site, like DGC2884 from *Pantoea* sp. YR343. Interestingly, multiple sequence alignments using protein sequences in Clustal Omega show a 33% sequence identity to TpbB from *P. aeruginosa* and 37% sequence identity to DgcN from *E. coli* (S5 Fig) [44]. Furthermore, YfiN in *P. aeruginosa* and *E. coli* is found within the YfiBNR operon, which consists of the outer membrane lipoprotein YfiB, which stimulates YfiN, and the soluble periplasmic protein YfiR, which represses the activity of YfiN [41,42]. Interestingly, DGC2884 is located within an operon that resembles the YfiBNR operon, suggesting that some parallels can be drawn. For example, YfiN in *P. aeruginosa*, *E. coli*, and *S. enterica* have each been shown to impact production of small colony variants, swimming motility and EPS production, similar to DGC2884 [42,43]. Interestingly, YfiN has been shown to modulate production of Psl polysaccharides, whose operon possesses genes also found to regulate amylovoran biosynthesis in *Erwinia amylovora* [41,42,45]. While the specific stimuli for each of these enzymes is not yet known, some studies suggest a reductive or osmotic stress may serve as an input to this system [41,42,46]. This may imply that the chemical environment of the rhizosphere induces expression of this diguanylate cyclase; however, further experimentation is required to test this. Further studies of enzymes like DGC2884 may provide important insights into the functions of both medically-important and agriculturally important microbes, such as the closely related pathogens *Erwinia amylovora* or *Pantoea stewartii* [47,48].

Transposon mutagenesis of *Pantoea* sp. YR343 (pSRK-*DGC2884*) resulted in 136 mutants that affected a total of 58 genes identified from a small-scale library consisting of approximately 5,000 different clones. Surprisingly, approximately one-third of these mutants were affected in a component of the flagellar export apparatus, *fliR*, and we are currently investigating the role of this protein in relation to DGC2884. Although we obtained a wide selection of mutants, the conditions of our mutagenesis assay likely did not reach saturation, yielding the possibility that there are other genes of interest that have not yet been identified. It should also be noted that the colony morphology screening criteria used for this study likely identified some mutants independent of their response to high c-di-GMP levels. More work is needed to determine whether there are relationships between the identified gene products, DGC2884, and c-di-GMP.

Among the transposon mutants described here, the UDP::Tn5 and CAP::Tn5 mutants each have predicted roles in exopolysaccharide biosynthesis and transport [49]. Exopolysaccharides are known to play an important role in biofilm formation and root colonization [50–52]. Many *Pantoea* species are associated with plants, some as pathogens while others appear to be beneficial [53]. Two closely related species, *P. stewartii* and *E. amylovora*, have been shown to produce specific types of EPS, known as stewartan and amylovoran, that are integral to their function as pathogens [48,54–56]. While studies of this EPS have focused primarily on its role in pathogenesis, we have not found any evidence to suggest that *Pantoea* sp. YR343 is pathogenic under the conditions tested [15]; rather, we have found that *Pantoea* sp. YR343 is a robust root colonizer and mutations affecting EPS result in a significant reduction in root colonization. We show here that the UDP::Tn5 mutant shows little observable root colonization, while the CAP::Tn5 mutant colonizes well, but in a pattern that differs significantly from the wild type. Interestingly, there were no indications of a colonization defect in the CAP::Tn5 mutant based on cell number per gram root; however, imaging studies indicated that the CAP::Tn5 mutant does not form patches of cell aggregates on the root surface, suggesting differences in the amount or composition of EPS in this mutant.

Our data shows an increase in root colonization by the Type VI::Tn5, ABC::Tn5, and Ndk::Tn5 mutants, although the increases were slight. Interestingly, the patterns of colonization in

the Ndk::Tn5 mutant were mostly in the form of small patches along the root surface, while colonization by the TypeVI::Tn5 and ABC::Tn5 mutants were observed as both small patches and long strips along the root hairs. Perhaps some of these gene products are involved in determining where to colonize the plant root, as well as pattern formation during root colonization. For example, the Type VI secretion system is believed to promote fitness and competition within the rhizosphere during root colonization [57]. Perhaps without this system, the cells are unable to colonize the older tissue along the primary plant root, but can better colonize the softer root hairs. More studies are required to understand how these different gene products are involved in regulating colonization behaviors.

Finally, the finding that at least three diguanylate cyclases were expressed during plant association suggests that c-di-GMP signaling is involved in root colonization by *Pantoea* sp. YR343. Characterizing the coordination of these three diguanylate cyclases in the process of root colonization by *Pantoea* sp. YR343 will enhance our understanding of c-di-GMP regulation across bacteria and yield important insights into the roles of multiple diguanylate cyclases in coordinating these behaviors.

Materials and methods

Bacterial strains and growth conditions

S1 Table describes the bacterial strains and plasmids used throughout this study. *E. coli* strains were grown in Luria Broth (LB) media (10 g Tryptone, 5 g Yeast Extract, and 10 g NaCl per 1 liter) with shaking at 37˚C. *Pantoea* strains were grown in either R2A broth (TEKnova, Inc.), LB, TY (10 g tryptone and 5 g yeast extract per 1 liter), or M9 media with 0.4% glucose and grown at 28˚C. Growth curve assays were performed using 96-well plates in a Biotek Cytation 5 plate reader. Motility assays were performed on low agar plates prepared by adding 0.3% agar to LB media. Congo Red plates (for EPS analysis) were prepared by adding Congo Red to R2A or LB media at a concentration of 40 μg ml^{-1}.

Construction of promoter-reporter plasmids

To generate reporter constructs, we analyzed the genomic sequences upstream of the predicted ATG start sites of each diguanylate cyclase in order to identify putative promoters using BPROM [22]. We then cloned 200 bp regions encoding the predicted promoters for use in the reporter construct, pPROBE-NT [21]. Primers used to amplify each of these promoter regions are listed in S2 Table. Final constructs were verified using restriction digests, prior to introduction into *Pantoea* sp. YR343 using electroporation.

Construction of diguanylate cyclase expression vectors

DGC2884 and DGC2884ΔTM were amplified by PCR from genomic DNA using the primers listed in S2 Table. PCR products were digested with BamHI and HindIII before ligation into pSRK-Km or pSRK-Gm [58]. The DGC2884 AADEF mutant was generated using a Quik-Change Site-directed mutagenesis kit, with the cloned wild type DGC2884 as a template, and the resulting construct was verified by sequencing. Each construct was verified before transforming into electrocompetent wild type *Pantoea* sp. YR343, as described previously [15]. Each overexpression strain was maintained with either 50 μg mL^{-1} kanamycin (pSRK-Km) or 10 μg mL^{-1} gentamycin (pSRK-Gm) and induction was performed by adding 1 mM isopropyl β-D-1-thiogalactopyranoside (IPTG).

Tagged diguanylate cyclases were generated by PCR amplification of each diguanylate cyclase followed by cloning into pENTR D-TOPO (ThermoFisher Scientific) and then

transferred to either pRH016 (HA tag) or pRH018 (Myc tag) [59]. Final constructs containing HA or Myc tags were then introduced into *Pantoea* YR343 via electroporation as described previously [15].

Biofilm formation assays

We tested biofilm formation on vinyl coverslips using cultures grown in M9 minimal media supplemented with 0.4% glucose. Coverslips were sterilized by soaking in 100% bleach for 20 minutes and then rinsed twice in sterile water before placing in a sterile 12-well tissue culture dish. Sterility was tested using sterile M9 media with 0.4% glucose with sterilized coverslips. Cultures were grown in M9 minimal media overnight, then diluted 1:100 into fresh M9 media with 0.4% glucose (1 mM IPTG was added for strains with pSRK). Diluted cultures (1 mL) were then placed into a 12-well tissue culture dish (three replicates per strain) along with a sterilized vinyl coverslip placed at an angle. A breathable cover was placed over the 12-well tissue culture dish and was placed at 28˚C for 72 hours. Coverslips were then removed and rinsed in water prior to staining with crystal violet as described previously [15]. Expression using GFP reporter strains was measured by rinsing coverslips and imaging large sections of biofilms over a minimum of three separate fields of view. Details of image analysis are described below.

Pellicle formation assays

Pellicle assays were performed as described previously [15]. In order to quantify the percentage of cells within each pellicle, we collected 100 μL of cells from the non-pellicle portion of each culture, then used a glass homogenizer to disperse the pellicle with the remaining culture. From the homogenized culture, we collected 100 μL of cells. The OD (600 nm) was measured for the homogenized culture, as well as the non-pellicle portion, in order to calculate the percentage of cells that were in the pellicle. There were three biological replicates measured per experiment. Expression using GFP reporter strains was measured by taking a small sample of cells from cultures grown as pellicles and measuring fluorescence, as well as cell density (OD at 600 nm) using the Biotek Cytation 5 plate reader. Fluorescence measurements were then normalized against cell density measurements.

Expression of diguanylate cyclases and enzyme assays using Vc2-Spinach

We obtained the pET31b-Vc2 Spinach vector as a gift from Dr. Ming Hammond and used *E. coli* BL21 DE3 Star cells to co-express the Vc2-Spinach tRNA (from pET31b-Vc2 Spinach) with each diguanylate cyclase construct (pSRK (Km) DGC2884, pSRK (Km) DGC2884 AADEF, pSRK (Km) and DGC2884ΔTM) individually as described previously [32]. We verified expression of each of these constructs by RT-PCR using protocols described below (see *Expression analysis*). Measurement of c-di-GMP using the Vc2-Spinach aptamer was performed as described previously [32].

Expression analysis

In order to ensure expression of diguanylate cyclase genes, we performed RT-PCR using primer sets for each diguanylate cyclase (primers listed in S2 Table). RNA extraction was performed using the Qiagen RNeasy Mini Kit according to manufacturer's protocols. The SuperScript IV RT-PCR system (ThermoFisher Scientific) was used for generating cDNA according to manufacturer's procedures and final PCR reactions were performed according to standard protocols.

Immunolocalization and Western blotting

Immunolocalization was performed on *Pantoea* sp. YR343 (pRH016-*DGC2884*) and YR343 (pRH018-*DGC2884ΔTM*) using mouse polyclonal antibodies against HA (ab16918 from Abcam) or Myc (13–2500 from Invitrogen). Approximately 3 mL of cell culture grown to a low cell density was collected, washed in PBS, and fixed in ice cold methanol for 1 hour at -20˚C. Afterwards, cells were placed onto poly-L-lysine coated coverslips and allowed to dry before lysing with 2 mg mL^{-1} lysozyme solution in GTE buffer (50 mM glucose, 20 mM Tris-HCl pH 8.0, 10 mM EDTA) for 10 minutes, followed by incubation overnight at 4˚C in a blocking solution consisting of 1% non-fat dry milk in PBS, pH 7.0. After washing twice with PBS, the antibody solution consisting of 1% non-fat dry milk in PBS with either 1:250 dilution of anti-HA or 1:125 dilution of anti-Myc antibody was added and incubated for 2 hrs at room temperature. The coverslips were rinsed in PBS and then incubated with Alexa Fluor 488 goat anti-mouse IgG at a 1:500 dilution in 1% non-fat dry milk in PBS for 2 hours at room temperature. Coverslips were washed in PBS, mounted on slides and imaged using a Zeiss LSM710 confocal microscope.

Lysates were prepared for western blotting by collecting cell pellets from cultures grown overnight, resuspended in PBS with 10% glycerol and 0.1% Triton X-100, then lysed by sonication at 50% amplitude with 10 second on/off cycles for a total of one minute. The crude lysate was centrifuged and supernatants were used for SDS-PAGE gels. Western blotting was performed according to standard protocols using the same mouse monoclonal antibodies used for immunolocalization at a 1:750 dilution and goat anti-mouse secondary antibody at 1:7500 [60]. Detection of bands was performed using a DAB-peroxidase substrate solution.

Transposon mutagenesis and rescue cloning

Biparental mating was used to introduce the plasmid pRL27, encoding a mini-Tn5 transposon, into *Pantoea* sp. YR343 (DGC2884 pSRK-Gm) essentially as described previously, but on a smaller scale [61]. Removal of *E. coli* strain EA145 was performed by growing *Pantoea* in the presence of kanamycin (50 μg mL^{-1}) and gentamycin (10 μg mL^{-1}). Screening of the transposon library was performed by plating the library onto LB plates containing Congo Red (40 μg ml^{-1}), 1 mM IPTG, kanamycin (50 μg mL^{-1}) and gentamycin (10 μg mL^{-1}). Colonies differing in appearance from the parental strain were isolated for further characterization and for sequencing.

In order to identify the location of transposon insertions, we used a cloning approach described previously [61]. Basically, we isolated genomic DNA from each mutant using the Promega Wizard Genomic DNA Extraction Kit, digested with a single restriction enzyme (most often used EcoRI, but sometimes used BamHI, PstI, SalI, SacII, and SphI) that does not cut within the transposon, ligated the DNA into plasmids, transformed these plasmids into *E. coli* PIR1 cells (ThermoFisher Scientific) and then plated onto selective plates containing 50 μg mL^{-1} kanamycin (transposon sequence contained a kanamycin resistance marker). Colonies were picked and plasmid DNA was isolated using the QIAprep Spin Miniprep Kit (Qiagen) and plasmids were sequenced at the Molecular Biology Resource Facility at the University of Tennessee, Knoxville. We sequenced each plasmid from the transposon outwards using the following primers, tpnRL17-1 and tpnRL13-1 [61]. All resulting sequences were analyzed using BlastX from NCBI in order to identify the region of DNA flanking each transposon.

Individual transposon mutants were grown three to four times sequentially on rich media without selection in order to remove the pSRK (Gm)-*DGC2884* plasmid. Removal of the plasmid was verified by growth on kanamycin at 50 μg mL^{-1}, but not on gentamycin at 10 μg mL^{-1}.

Construction of fluorescent strains. We generated fluorescent strains that were also resistant to gentamycin by integrating either GFP or mCherry into the chromosome of *Pantoea* sp. YR343 using the pBT270 and pBT277 plasmids which use the Tn7 transposon system for chromosomal insertions (gift from B.S. Tseng and [62]). Colonies with chromosomally inserted GFP or mCherry were selected on R2A agar containing gentamycin at 10 μg mL^{-1}.

Plant growth conditions and inoculation

Wheat seeds were grown in special growth chambers (Advanced Science Tools, LLC–http://advancedsciencetools.com/index.html) which allow for visualization of plant roots without sacrificing the plants. Wheat seeds were surface-sterilized, as performed previously [15] and placed into the chamber filled with sterile soil. Once seeds were germinated and had both stem and roots, plants were inoculated with *Pantoea* sp. YR343, as described previously [15]. Plants were incubated with *Pantoea* sp. YR343 for 7 days prior to visualization using confocal microscopy.

Colonization of *Populus trichocarpa* BESC819 was performed as described previously [15]. Five plants were used per treatment (with approximately 10^7 cells per plant) and incubations were for three weeks prior to harvesting and counting. Visualization of non-fluorescently labelled cells was performed by staining with Syto 9, as described previously [15].

Confocal fluorescence microscopy and image analysis

Biofilms were imaged for promoter expression analysis using a Biotek Cytation 5 plate reader. Images were taken from at least three separate fields-of-view per sample. In order to quantify fluorescence, we drew nine square regions of interest per image using Fiji ImageJ and measured fluorescence intensity per square for all images. The average fluorescence intensity per square micrometer, as well as the S.E.M. values were calculated for each sample and then normalized against the pPROBE empty vector control.

Confocal fluorescence microscopy was performed using a Zeiss LSM710 confocal laser scanning microscope with a Plan-Apochromat 63x/1.40 oil immersion objective (Carl Zeiss Microimaging, Thornwood, NY). Images were processed using Zen2012 software (Zeiss). Cell fluorescence intensity measurements were performed using Fiji ImageJ for assays with promoter-reporter fusions for DGCs and for the Vc2 Spinach aptamer following the protocol described by Kellenberger, et al [32]. Briefly, images were initially collected using the same parameters and then collectively processed so that brightness and contrast was adjusted and normalized across the entire set of images used for analysis. Using brightfield images, individual regions-of-interest were drawn for a minimum of 50 cells, then used to measure fluorescence in corresponding fluorescent images.

Statistical analysis

In datasets with statistical analysis using either a student's t-test or ANOVA, we used the Data Analysis ToolPak add-on in Microsoft Excel 2016, as part of Microsoft Office 365. T-test measurements were done as "two sample assuming equal variances" with an alpha value of 0.05 and one-tail p-values were calculated. ANOVA analysis was performed across groups of data as "single factor ANOVA" with an alpha value of 0.05.

Supporting information

S1 Fig. Growth curves of wild type (pSRK-Km) and the indicated DGC overexpressing strains in minimal media (A) and LB media (B). Error bars represent the standard deviation from

three independent cultures.
(TIF)

S2 Fig. Expression of individual diguanylate cyclases using RT-PCR. Image shown is representative of a minimum of 3 replicates.
(TIF)

S3 Fig. Western blot showing expression of tagged full length DGC2884 and DGC2884ΔTM. Weights of markers are indicated on the left and arrows point to bands that represent the indicated protein.
(TIF)

S4 Fig. Growth curves of wild type Pantoea sp. YR343 and indicated transposon mutants in minimal media (A) and in LB media (B). Error bars represent the standard deviation from three independent cultures.
(TIF)

S5 Fig. Clustal Omega multiple sequence alignment of *Pantoea* sp. YR343 DGC2884, *Pseudomonas aeruginosa* PA01 TpbB, and *Escherichia coli* MG1655 DgcN [44].
(TIF)

S1 Table. Strains and plasmids used in this study.
(PDF)

S2 Table. Primers used in this study.
(PDF)

S1 Raw images. Original gel and Western blot images corresponding to S2 and S3 Figs.
(PDF)

Acknowledgments

We would like to thank Dr. B. S. Tseng (University of Washington) for sharing plasmids pBT270 and pBT277, as well as Dr. Alison Buchan (University of Tennessee, Knoxville) for sharing the pRL27 plasmid, and finally, Dr. Ming Hammond (University of Utah) for sharing pET31b-Vc2 Spinach.

Author Contributions

Conceptualization: Jennifer L. Morrell-Falvey.

Investigation: Amber N. Bible, Mang Chang.

Methodology: Amber N. Bible, Jennifer L. Morrell-Falvey.

Supervision: Jennifer L. Morrell-Falvey.

Validation: Amber N. Bible, Jennifer L. Morrell-Falvey.

Writing – original draft: Amber N. Bible.

Writing – review & editing: Mang Chang, Jennifer L. Morrell-Falvey.

References

1. Hengge R. Principles of c-di-GMP signalling in bacteria. Nature reviews Microbiology. 2009; 7(4):263–73. https://doi.org/10.1038/nrmicro2109 PMID: 19287449

2. Jenal U, Malone J. Mechanisms of cyclic-di-GMP signaling in bacteria. Annu Rev Genet. 2006; 40:385–407. https://doi.org/10.1146/annurev.genet.40.110405.090423 PMID: 16895465
3. Romling U, Galperin MY, Gomelsky M. Cyclic di-GMP: the first 25 years of a universal bacterial second messenger. Microbiol Mol Biol Rev. 2013; 77(1):1–52. https://doi.org/10.1128/MMBR.00043-12 PMID: 23471616
4. Valentini M, Filloux A. Biofilms and Cyclic di-GMP (c-di-GMP) Signaling: Lessons from *Pseudomonas aeruginosa* and other bacteria. The Journal of biological chemistry. 2016; 291(24):12547–55. https://doi.org/10.1074/jbc.R115.711507 PMID: 27129226
5. Sondermann H, Shikuma NJ, Yildiz FH. You've come a long way: c-di-GMP signaling. Current opinion in microbiology. 2012; 15(2):140–6. https://doi.org/10.1016/j.mib.2011.12.008 PMID: 22226607
6. Kalia D, Merey G, Nakayama S, Zheng Y, Zhou J, Luo Y, et al. Nucleotide, c-di-GMP, c-di-AMP, cGMP, cAMP,(p) ppGpp signaling in bacteria and implications in pathogenesis. Chemical Society Reviews. 2013; 42(1):305–41. https://doi.org/10.1039/c2cs35206k PMID: 23023210
7. Boehm A, Kaiser M, Li H, Spangler C, Kasper CA, Ackermann M, et al. Second messenger-mediated adjustment of bacterial swimming velocity. Cell. 2010; 141(1):107–16. https://doi.org/10.1016/j.cell.2010.01.018 PMID: 20303158
8. Paul K, Nieto V, Carlquist WC, Blair DF, Harshey RM. The c-di-GMP binding protein YcgR controls flagellar motor direction and speed to affect chemotaxis by a "backstop brake" mechanism. Mol Cell. 2010; 38(1):128–39. https://doi.org/10.1016/j.molcel.2010.03.001 PMID: 20346719
9. Krasteva PV, Fong JC, Shikuma NJ, Beyhan S, Navarro MV, Yildiz FH, et al. *Vibrio cholerae* VpsT regulates matrix production and motility by directly sensing cyclic di-GMP. science. 2010; 327(5967):866–8. https://doi.org/10.1126/science.1181185 PMID: 20150502
10. Ryjenkov DA, Simm R, Romling U, Gomelsky M. The PilZ domain is a receptor for the second messenger c-di-GMP: the PilZ domain protein YcgR controls motility in enterobacteria. The Journal of biological chemistry. 2006; 281(41):30310–4. https://doi.org/10.1074/jbc.C600179200 PMID: 16920715
11. Amikam D, Galperin MY. PilZ domain is part of the bacterial c-di-GMP binding protein. Bioinformatics. 2006; 22(1):3–6. https://doi.org/10.1093/bioinformatics/bti739 PMID: 16249258
12. Fang X, Ahmad I, Blanka A, Schottkowski M, Cimdins A, Galperin MY, et al. GIL, a new c-di-GMP-binding protein domain involved in regulation of cellulose synthesis in enterobacteria. Molecular microbiology. 2014; 93(3):439–52. https://doi.org/10.1111/mmi.12672 PMID: 24942809
13. Sudarsan N, Lee ER, Weinberg Z, Moy RH, Kim JN, Link KH, et al. Riboswitches in eubacteria sense the second messenger cyclic di-GMP. Science. 2008; 321(5887):411–3. https://doi.org/10.1126/science.1159519 PMID: 18635805
14. Christen B, Christen M, Paul R, Schmid F, Folcher M, Jenoe P, et al. Allosteric control of cyclic di-GMP signaling. The Journal of biological chemistry. 2006; 281(42):32015–24. https://doi.org/10.1074/jbc.M603589200 PMID: 16923812
15. Bible AN, Fletcher SJ, Pelletier DA, Schadt CW, Jawdy SS, Weston DJ, et al. A carotenoid-deficient mutant in *Pantoea* sp. YR343, a bacteria isolated from the rhizosphere of *Populus deltoides*, is defective in root colonization. Frontiers in microbiology. 2016; 7:491. https://doi.org/10.3389/fmicb.2016.00491 PMID: 27148182
16. Cregger M, Carper DL, Christel S, Doktycz M, Labbe J, Michener J, et al. Plant-microbe interactions: from genes to ecosystems using *Populus* as a model system. Phytobiomes Journal. 2021(ja).
17. Estenson K, Hurst GB, Standaert RF, Bible AN, Garcia D, Chourey K, et al. Characterization of indole-3-acetic acid biosynthesis and the effects of this phytohormone on the proteome of the plant-associated microbe *Pantoea* sp. YR343. Journal of proteome research. 2018. https://doi.org/10.1021/acs.jproteome.7b00708 PMID: 29464956
18. Garcia DC, Cheng X, Land ML, Standaert RF, Morrell-Falvey JL, Doktycz MJ. Computationally guided discovery and experimental validation of indole-3-acetic acid synthesis pathways. ACS chemical biology. 2019; 14(12):2867–75. https://doi.org/10.1021/acschembio.9b00725 PMID: 31693336
19. Lugtenberg B, Kamilova F. Plant-growth-promoting rhizobacteria. Annu Rev Microbiol. 2009; 63:541–56. https://doi.org/10.1146/annurev.micro.62.081307.162918 PMID: 19575558
20. El-Gebali S, Mistry J, Bateman A, Eddy SR, Luciani A, Potter SC, et al. The Pfam protein families database in 2019. Nucleic Acids Res. 2018; 47(D1):D427–D32.
21. Miller WG, Leveau JH, Lindow SE. Improved gfp and inaZ broad-host-range promoter-probe vectors. Mol Plant Microbe Interact. 2000; 13(11):1243–50. https://doi.org/10.1094/MPMI.2000.13.11.1243 PMID: 11059491
22. Solovyev V. V. Solovyev, A Salamov (2011) Automatic annotation of microbial genomes and metagenomic sequences. In Metagenomics and its Applications in Agriculture, Biomedicine and Environmental Studies (Ed. R.W. Li), Nova Science Publishers, p.61-78. 2011. p. 61–78.

23. Yang CY, Chin KH, Chuah ML, Liang ZX, Wang AH, Chou SH. The structure and inhibition of a GGDEF diguanylate cyclase complexed with (c-di-GMP)(2) at the active site. Acta Crystallogr D Biol Crystallogr. 2011; 67(Pt 12):997–1008. https://doi.org/10.1107/S090744491104039X PMID: 22120736

24. Malone JG, Williams R, Christen M, Jenal U, Spiers AJ, Rainey PB. The structure-function relationship of WspR, a *Pseudomonas fluorescens* response regulator with a GGDEF output domain. Microbiology (Reading, England). 2007; 153(Pt 4):980–94. https://doi.org/10.1099/mic.0.2006/002824-0 PMID: 17379708

25. Al-Bassam MM, Haist J, Neumann SA, Lindenberg S, Tschowri N. Expression patterns, genomic conservation and input into developmental regulation of the GGDEF/EAL/HD-GYP domain proteins in Streptomyces. Frontiers in microbiology. 2018; 9:2524. https://doi.org/10.3389/fmicb.2018.02524 PMID: 30405580

26. den Hengst CD, Tran NT, Bibb MJ, Chandra G, Leskiw BK, Buttner MJ. Genes essential for morphological development and antibiotic production in *Streptomyces coelicolor* are targets of BldD during vegetative growth. Molecular microbiology. 2010; 78(2):361–79. https://doi.org/10.1111/j.1365-2958.2010.07338.x PMID: 20979333

27. Purcell EB, McKee RW, McBride SM, Waters CM, Tamayo R. Cyclic diguanylate inversely regulates motility and aggregation in *Clostridium difficile*. J Bacteriol. 2012; 194(13):3307–16. https://doi.org/10.1128/JB.00100-12 PMID: 22522894

28. Waters CM, Lu W, Rabinowitz JD, Bassler BL. Quorum sensing controls biofilm formation in *Vibrio cholerae* through modulation of cyclic di-GMP levels and repression of *vpsT*. J Bacteriol. 2008; 190(7):2527–36. https://doi.org/10.1128/JB.01756-07 PMID: 18223081

29. Wood PJ, Flucher RG. Interaction of some dyes with cereal beta-glucans. Cereal Chemistry. 1978; 55(6):952–66.

30. Wolfe AJ, Visick KL. Get the message out: cyclic-di-GMP regulates multiple levels of flagellum-based motility. J Bacteriol. 2008; 190(2):463–75. https://doi.org/10.1128/JB.01418-07 PMID: 17993515

31. Römling U, Amikam D. Cyclic di-GMP as a second messenger. Current opinion in microbiology. 2006; 9(2):218–28. https://doi.org/10.1016/j.mib.2006.02.010 PMID: 16530465

32. Kellenberger CA, Wilson SC, Sales-Lee J, Hammond MC. RNA-based fluorescent biosensors for live cell imaging of second messengers cyclic di-GMP and cyclic AMP-GMP. J Am Chem Soc. 2013; 135(13):4906–9. https://doi.org/10.1021/ja311960g PMID: 23488798

33. Noirot-Gros MF, Shinde S, Larsen PE, Zerbs S, Korajczyk PJ, Kemner KM, et al. Dynamics of aspen roots colonization by pseudomonads reveals strain-specific and mycorrhizal-specific patterns of biofilm formation. Frontiers in microbiology. 2018; 9:853. https://doi.org/10.3389/fmicb.2018.00853 PMID: 29774013

34. Engl C, Waite CJ, McKenna JF, Bennett MH, Hamann T, Buck M. Chp8, a diguanylate cyclase from Pseudomonas syringae pv. Tomato DC3000, suppresses the pathogen-associated molecular pattern flagellin, increases extracellular polysaccharides, and promotes plant immune evasion. MBio. 2014; 5(3):e01168–14. https://doi.org/10.1128/mBio.01168-14 PMID: 24846383

35. Jones JDG, Dangl JL. The plant immune system. Nature. 2006; 444(7117):323–9. https://doi.org/10.1038/nature05286 PMID: 17108957

36. Pfeilmeier S, Saur IM, Rathjen JP, Zipfel C, Malone JG. High levels of cyclic-di-GMP in plant-associated *Pseudomonas* correlate with evasion of plant immunity. Mol Plant Pathol. 2016; 17(4):521–31. https://doi.org/10.1111/mpp.12297 PMID: 26202381

37. Taylor BL, Zhulin IB. PAS Domains: Internal sensors of oxygen, redox potential, and light. Microbiology and Molecular Biology Reviews. 1999; 63(2):479–506. https://doi.org/10.1128/MMBR.63.2.479-506.1999 PMID: 10357859

38. Zhulin IB, Nikolskaya AN, Galperin MY. Common extracellular sensory domains in transmembrane receptors for diverse signal transduction pathways in Bacteria and Archaea. J Bacteriol. 2003; 185(1):285–94. https://doi.org/10.1128/JB.185.1.285-294.2003 PMID: 12486065

39. Anantharaman V, Aravind L. The CHASE domain: a predicted ligand-binding module in plant cytokinin receptors and other eukaryotic and bacterial receptors. Trends Biochem Sci. 2001; 26(10):579–82. https://doi.org/10.1016/s0968-0004(01)01968-5 PMID: 11590000

40. Nikolskaya AN, Mulkidjanian AY, Beech IB, Galperin MY. MASE1 and MASE2: two novel integral membrane sensory domains. J Mol Microbiol Biotechnol. 2003; 5(1):11–6. https://doi.org/10.1159/000068720 PMID: 12673057

41. Malone JG, Jaeger T, Manfredi P, Dötsch A, Blanka A, Bos R, et al. The YfiBNR signal transduction mechanism reveals novel targets for the evolution of persistent *Pseudomonas aeruginosa* in Cystic Fibrosis airways. PLOS Pathogens. 2012; 8(6):e1002760. https://doi.org/10.1371/journal.ppat.1002760 PMID: 22719254

42. Malone JG, Jaeger T, Spangler C, Ritz D, Spang A, Arrieumerlou C, et al. YfiBNR mediates cyclic di-GMP dependent small colony variant formation and persistence in Pseudomonas aeruginosa. PLoS Pathog. 2010; 6(3):e1000804. https://doi.org/10.1371/journal.ppat.1000804 PMID: 20300602

43. Kim HK, Harshey RM. A diguanylate cyclase acts as a cell division inhibitor in a two-step response to reductive and envelope stresses. mBio. 2016; 7(4):e00822–16. https://doi.org/10.1128/mBio.00822-16 PMID: 27507823

44. Madeira F, Park YM, Lee J, Buso N, Gur T, Madhusoodanan N, et al. The EMBL-EBI search and sequence analysis tools APIs in 2019. Nucleic Acids Res. 2019; 47(W1):W636–W41. https://doi.org/10.1093/nar/gkz268 PMID: 30976793

45. Jackson KD, Starkey M, Kremer S, Parsek MR, Wozniak DJ. Identification of *psl*, a locus encoding a potential exopolysaccharide that is essential for *Pseudomonas aeruginosa* PAO1 biofilm formation. J Bacteriol. 2004; 186(14):4466–75. https://doi.org/10.1128/JB.186.14.4466-4475.2004 PMID: 15231778

46. Giardina G, Paiardini A, Fernicola S, Franceschini S, Rinaldo S, Stelitano V, et al. Investigating the allosteric regulation of YfiN from *Pseudomonas aeruginosa*: clues from the structure of the catalytic domain. PloS one. 2013; 8(11):e81324. https://doi.org/10.1371/journal.pone.0081324 PMID: 24278422

47. Falkenstein H, Bellemann P, Walter S, Zeller W, Geider K. Identification of *Erwinia amylovora*, the fireblight pathogen, by colony hybridization with DNA from plasmid pEA29. Appl Environ Microbiol. 1988; 54 (11):2798–802. https://doi.org/10.1128/aem.54.11.2798-2802.1988 PMID: 16347778

48. Roper MC. *Pantoea stewartii* subsp. *stewartii*: lessons learned from a xylem-dwelling pathogen of sweet corn. Molecular plant pathology. 2011; 12(7):628–37. https://doi.org/10.1111/j.1364-3703.2010.00698.x PMID: 21726365

49. Bernhard F, Coplin DL, Geider K. A gene cluster for amylovoran synthesis in *Erwinia amylovora*: characterization and relationship to *cps* genes in *Erwinia stewartii*. Molecular and General Genetics MGG. 1993; 239(1):158–68. https://doi.org/10.1007/BF00281614 PMID: 8389975

50. Danhorn T, Fuqua C. Biofilm formation by plant-associated bacteria. Annu Rev Microbiol. 2007; 61:401–22. https://doi.org/10.1146/annurev.micro.61.080706.093316 PMID: 17506679

51. Ramey BE, Koutsoudis M, von Bodman SB, Fuqua C. Biofilm formation in plant-microbe associations. Current opinion in microbiology. 2004; 7(6):602–9. https://doi.org/10.1016/j.mib.2004.10.014 PMID: 15556032

52. Castiblanco LF, Sundin GW. New insights on molecular regulation of biofilm formation in plant-associated bacteria. Journal of integrative plant biology. 2016; 58(4):362–72. https://doi.org/10.1111/jipb.12428 PMID: 26377849

53. Walterson AM, Stavrinides J. *Pantoea*: insights into a highly versatile and diverse genus within the *Enterobacteriaceae*. FEMS microbiology reviews. 2015; 39(6):968–84. https://doi.org/10.1093/femsre/fuv027 PMID: 26109597

54. Koutsoudis MD, Tsaltas D, Minogue TD, von Bodman SB. Quorum-sensing regulation governs bacterial adhesion, biofilm development, and host colonization in *Pantoea stewartii* subspecies *stewartii*. Proceedings of the National Academy of Sciences of the United States of America. 2006; 103(15):5983–8. https://doi.org/10.1073/pnas.0509860103 PMID: 16585516

55. Geider K. Exopolysaccharides of Erwinia amylovora: Structure, Biosynthesis, Regulation, Role in Pathogenicity of. Fire blight: the disease and its causative agent, Erwinia amylovora. 2000:117.

56. Koczan JM, McGrath MJ, Zhao Y, Sundin GW. Contribution of *Erwinia amylovora* exopolysaccharides amylovoran and levan to biofilm formation: implications in pathogenicity. Phytopathology. 2009; 99 (11):1237–44. https://doi.org/10.1094/PHYTO-99-11-1237 PMID: 19821727

57. Bernal P, Llamas MA, Filloux A. Type VI secretion systems in plant-associated bacteria. Environmental microbiology. 2018; 20(1):1–15. https://doi.org/10.1111/1462-2920.13956 PMID: 29027348

58. Khan SR, Gaines J, Roop RM, Farrand SK. Broad-Host-Range expression vectors with tightly regulated promoters and their use to examine the influence of TraR and TraM expression on Ti plasmid quorum sensing. Applied and environmental microbiology. 2008; 74(16):5053–62. https://doi.org/10.1128/AEM.01098-08 PMID: 18606801

59. Hallez R, Letesson JJ, Vandenhaute J, De Bolle X. Gateway-based destination vectors for functional analyses of bacterial ORFeomes: application to the Min system in *Brucella abortus*. Applied and environmental microbiology. 2007; 73(4):1375–9. https://doi.org/10.1128/AEM.01873-06 PMID: 17172460

60. Mahmood T, Yang PC. Western blot: technique, theory, and trouble shooting. North American journal of medical sciences. 2012; 4(9):429–34. https://doi.org/10.4103/1947-2714.100998 PMID: 23050259

61. Larsen RA, Wilson MM, Guss AM, Metcalf WW. Genetic analysis of pigment biosynthesis in *Xanthobacter autotrophicus* Py2 using a new, highly efficient transposon mutagenesis system that is functional in a wide variety of bacteria. Archives of microbiology. 2002; 178(3):193–201. https://doi.org/10.1007/s00203-002-0442-2 PMID: 12189420

62. Zhao K, Tseng BS, Beckerman B, Jin F, Gibiansky ML, Harrison JJ, et al. Psl trails guide exploration and microcolony formation in *Pseudomonas aeruginosa* biofilms. Nature. 2013; 497:388. https://doi.org/10.1038/nature12155 PMID: 23657259